Bioactive Materials 9 (2022) 29–43

Contents lists available at ScienceDirect

Bioactive Materials

journal homepage: www.sciencedirect.com/journal/bioactive-materials

Injectable self-healing hydrogel with siRNA delivery property for sustained STING silencing and enhanced therapy of intervertebral disc degeneration

Jiaxin Chen [a,1], Haifeng Zhu [a,1], Yutao Zhu [a], Chenchen Zhao [a], Shengyu Wang [a], Yixin Zheng [a], Ziang Xie [a], Yang Jin [a], Honghai Song [a], Linjun Yang [a], Jin Zhang [b,*], Jiayong Dai [a,**], Zhijun Hu [a,***], Huaiyu Wang [c]

[a] Department of Orthopaedic Surgery, Sir Run Run Shaw Hospital, Zhejiang University School of Medicine, Key Laboratory of Musculoskeletal System Degeneration, Regeneration Translational Research of Zhejiang Province, East Qing Chun Road, Hangzhou, 310016, PR China
[b] College of Chemical Engineering, Fuzhou University, 2 Xueyuan Road, Fuzhou, 350108, PR China
[c] Center for Human Tissues and Organs Degeneration, Shenzhen Institutes of Advanced Technology, Chinese Academy of Sciences, Shenzhen, 518055, Guangdong, PR China

ARTICLE INFO

Keywords:
STING
IVD degeneration
siRNA delivery
Injectable hydrogel
Dynamic Schiff base

ABSTRACT

Inflammatory responses of nucleus pulposus (NP) can induce imbalanced anabolism and catabolism of extracellular matrix, and the cytosolic dsDNA accumulation and STING–NF–κB pathway activation found in NP inflammation are considered as fairly important cause of intervertebral disc (IVD) degeneration. Herein, we constructed a siSTING delivery hydrogel of aldehyde hyaluronic acid (HA-CHO) and poly(amidoamine) PAMAM/siRNA complex to intervene the abnormal STING signal for IVD degeneration treatment, where the formation of dynamic Schiff base bonds in the system (siSTING@HP^{gel}) was able to overcome the shortcomings such as low cellular uptake, short half-life, and rapid degradation of siRNA-based strategy. PAMAM not only formed complexes with siRNA to promote siRNA transfection, but also served as dynamic crosslinker to construct hydrogel, and the injectable and self-healing hydrogel efficiently and steadily silenced STING expression in NP cells. Finally, the siSTING@HP^{gel} significantly eased IVD inflammation and slowed IVD degeneration by prolonging STING knockdown in puncture-induced IVD degeneration rat model, revealing that STING pathway was a therapeutic target for IVD degeneration and such novel hydrogel had great potential for being applied to many other diseases for gene delivery.

1. Introduction

Low back pain is a major cause of disability worldwide with a prevalence of over 80% and impact amounting to over one hundred billion dollars annually in direct and associated costs [1,2]. Primarily, intervertebral disc (IVD) degeneration is the causative factor of low back pain [3], and a multifactorial condition caused by aging, genetics, biomechanics, and environmental factors, whose hallmarks are the dysfunction of nucleus pulposus (NP) cells and disruption of the equilibrium between the anabolism and catabolism of the extracellular matrix (ECM) [4,5]. It has been reported that inflammatory response was implicated in the pathogenesis of IVD degeneration [6,7]. During the process of degeneration, the centrally located NP cells undergo phenotypic transition, resulting in increased production of pro-inflammatory cytokines including IL-6, IL-8, which mediates catabolism and anti-anabolic metabolism inside the NP cells and participates greatly in the establishment and progression of degeneration state of IVD [8]. Currently, the main challenges are the lack of knowledge of molecule mechanisms and pathways that involved in NP cells inflammation driving ECM destruction and the absence of appropriate strategy to intervene precisely in abnormal signals.

Stimulator of interferon genes (STING), an endoplasmic reticulum

Peer review under responsibility of KeAi Communications Co., Ltd.
* Corresponding author.
** Corresponding author.
*** Corresponding author.
E-mail addresses: J_Zhang929@fzu.edu.cn (J. Zhang), daijy@zju.edu.cn (J. Dai), hzjspine@zju.edu.cn (Z. Hu).
[1] J. Chen and H. Zhu contributed equally to this work.

https://doi.org/10.1016/j.bioactmat.2021.08.003
Received 21 May 2021; Received in revised form 4 August 2021; Accepted 4 August 2021
Available online 10 August 2021
2452-199X/© 2021 The Authors. Publishing services by Elsevier B.V. on behalf of KeAi Communications Co. Ltd. This is an open access article under the CC BY-NC-ND license (http://creativecommons.org/licenses/by-nc-nd/4.0/).

(ER) localized adaptor that senses cyclic dinucleotides from bacterial sources or cyclic GMP-AMP (cGAMP) produced by the cytosolic DNA sensor cyclic GMP-AMP synthase (cGAS), is originally discovered as an important molecule in immunity that detects DNA from infected pathogens and triggers the immune response [9–13]. Recently, accumulating evidence suggests a pathogenic role of STING in a range of inflammatory and degenerative diseases [14–20]. Self-DNA from mitochondrial DNA (mtDNA) or nucleus DNA aberrantly accumulate in the cytosol and gain access to trigger STING activation in diseases [21]. Upon activation, STING recruits TANK binding kinase 1 (TBK1), which phosphorylates transcription factors such as interferon regulatory factor 3 (IRF3) and nuclear factor-kappa B (NF-κB), to induce the production of type I interferons (IFNs) and proinflammatory cytokines including tumor necrosis factor-α (TNF-α), interleukin-1β (IL-1β) and IL-6 [22]. Previous study has reported that cisplatin exposure of human NP cells caused DNA damage and elevated cellular senescence and catabolism, by activating NF-κB signaling, and the DNA repair-deficient mouse model also exhibited loss of matrix proteoglycan and reduced IVD height [23]. However, the role of accumulation of cytoplasmic DNA and the function of STING in IVD inflammation has been rarely reported. Based on the well-established function of STING signaling in many other inflammation-related disorders and the involvement of DNA damage in IVD degeneration, we hypothesized that targeting STING might be a promising therapeutic strategy for preventing IVD inflammation and degeneration.

The effect of small interfering RNA (siRNA) to silence specific genes post-transcriptionally through degradation of the corresponding messenger RNA (mRNA) has emerged as a research tool and therapeutic agent for a broad range of diseases [24,25]. But, as anionic macromolecules, RNA molecules cannot easily traverse the plasma membrane and its degradation by endogenous ribonucleases (RNases) especially *in vivo* no doubt limits its utilization [26]. The rapid development of nanotechnology has led to a mass of nanocarriers being explored for siRNA delivery to enhance cellular uptake and improve RNA stability [27,28]. Even so, these systems suffer from typical nanocarriers' shortcomings of fast clearance. Importantly, short half-life of siRNA necessitates higher loading concentrations or more frequent administrations, which potentially increases cost and toxicity. As IVD is the most avascular tissue in the body, systemic delivery strategy may cause low residual concentration of drugs in IVD and results in little therapeutic effect [29]. Alternatively, local intervertebral injection for better keeping siRNA at the site of action is considered as an effective therapy approach. To obtain long-term effects, repeated multiple injections becomes necessary, while irreparable disc damage caused by excessive puncture injections seriously limits its application [30]. Designing siRNA carrier with properties of intensively transmitting high concentrations of siRNA to a target site and functioning for a sufficient time has been greatly urged. Among the carriers, hydrogel delivery platforms draw attention for localization possibilities, sustained, and prolonged release of siRNA to a target tissue [31]. Particularly, some injectable hydrogels have been developed to be used as minimally invasive therapy and they can also easily deliver siRNA to the complex contour of tissue sites [32,33]. However, the lack of self-healing capability of these hydrogels raises obstacles for the IVD treatment, since local high stress of disc space may break hydrogels into small fragments and may prematurely release or leak the encapsulated siRNA [34]. Together, ideal hydrogel carrier delivery siRNA for IVD degeneration needs to satisfy four following characters: (1) robust gene silencing efficacy; (2) sustained siRNA release for prolonged effect; (3) injectable property for minimally invasive purpose; (4) self-healing capability for resistance of broken.

In this work, the surgical IVD specimens were firstly analyzed and gene silence with commercial Lipofectamine 3000 transfection reagent in NP cells was conducted. We proved that STING functioned as the DNA sensor induced NF-κB dependent inflammation and degeneration in IVD. Based on the key role of STING in IVD degeneration, we designed a novel injectable, self-healing hydrogel delivery platform to transport siSTING for sustained gene silencing and enhanced therapy of IVD degeneration. The hydrogel was consisted of natural ECM component hyaluronic acids (HA) and gene carrier Amine-terminated Generation 5 (G5) poly(amidoamine) (PAMAM) dendrimers. The aldehyde-functionalized HA (HA-CHO) was synthesized through oxidation, and then the injectable hydrogel (siRNA@HP^{gel}) was prepared in a facile approach by mixing the solutions of HA-CHO and PAMAM/siRNA complexes through the formation of dynamic Schiff base bonds. HA was chosen as aldehyde-functionalized polymer chain due to its excellent biocompatible, while PAMAM not only formed complex with siRNA to promote siRNA transfection, but also served as dynamic crosslinker to construct hydrogel. In addition, PAMAM/siRNA complexes with robust gene silencing efficacy prolonged the release by dissociation from Schiff base bonds. Finally, siSTING@HP^{gel} was able to provide a sustained release of siSTING for the topical therapy of IVD degeneration in puncture-induced rat disc degeneration model (Scheme 1). The findings presented here provided new insights into the mechanism of IVD inflammatory degeneration and the established hydrogel delivery platform may be applied to other minimally-invasive treatment of gene expression related diseases.

2. Experimental Section

2.1. Materials

Amine-terminated G5 PAMAM was purchased from Dendritech (Midland, MI). sodium hyaluronate (100–150 kDa) was from Yuanye Bio-Technology Co. Ltd (Shanghai, China). Sodium periodate (ACS, 99.8%) and ethylene glycol were purchased from Aladdin (Shanghai, China). Dialysis tubing with 3500 molecular weight cut-off (MWCO) and CCK-8 kit were sourced from Solarbio (Beijing, China). Dulbecco's modified Eagle's medium and Ham's F-12 medium (DMEM/F12) and fetal bovine serum (FBS) were obtained from Gibco (Carlsbad, CA). 4′,6-diamidino-2-phenylindole (DAPI), Hoechst and the Live/Dead kit were purchased from Beyotime (Shanghai, China). Cell Fractionation Kit (ab109719) and antibodies of collagen II (ab34712), Mmp3 (ab52915), Mmp13 (ab51072), Tommo20 (ab186735) and dsDNA (ab27156) were purchased from Abcam (Cambridge, UK). The antibodies of STING (#13647), p-TBK1 (#5483), TBK1 (#38066), p-p65 (#3033), p65 (#8242) were from Cell Signaling (Shanghai, China). The antibodies of β-Actin (66009-1-Ig), GAPDH (60004-1-Ig), TNF-α (60291-1-Ig), IL-1β (16806-1-AP) and IL-6 (21865-1-AP) were obtained from Proteintech (Wuhan, China). The antibody of Aggrecan (A8536) was purchased from ABclonal (Wuhan, China). Specificity of all antibodies has been validated by the manufacturers using negative control IgG. Negative control siRNA, siSTING, cy3-siSTING, cy5-siSTING were purchased from GenePharma (Shanghai China) and the siRNA sequences were displayed in Table S2, Supporting Information. Lipofectamine 3000 siRNA transfection system were obtained from Thermo Fisher (UT, USA). QIAmp DNA Mini Kit, RNeasy Mini kit and HiFiScript cDNA kit was obtained from CWBio (Beijing, China). SYBR Green Master Mix was purchased from Yeasen Biotech Co. Ltd (Shanghai, China). All the reagents were used as received without further purification.

2.2. Surface modification of HA with aldehyde groups

HA-CHO was prepared by oxidation with sodium periodate. 2.0 g of high molecular mass hyaluronate sodium (5 mmol) was dissolved in 100 mL distilled water at a concentration of 2% (*W/V*). 1.08 g of sodium periodate (5 mmol) was dissolved in 6 mL distilled water then added dropwise to the HA solution in dark through vigorous stirring for 4 h at room temperature. Afterwards, 1 mL ethylene glycol was added to neutralize any unreacted periodate for 1 h. The HA-CHO was purified by dialysis with deionized water for 3 days and then lyophilized. The oxidation degree of HA was evaluated through hydroxylamine hydrochloride method [35].

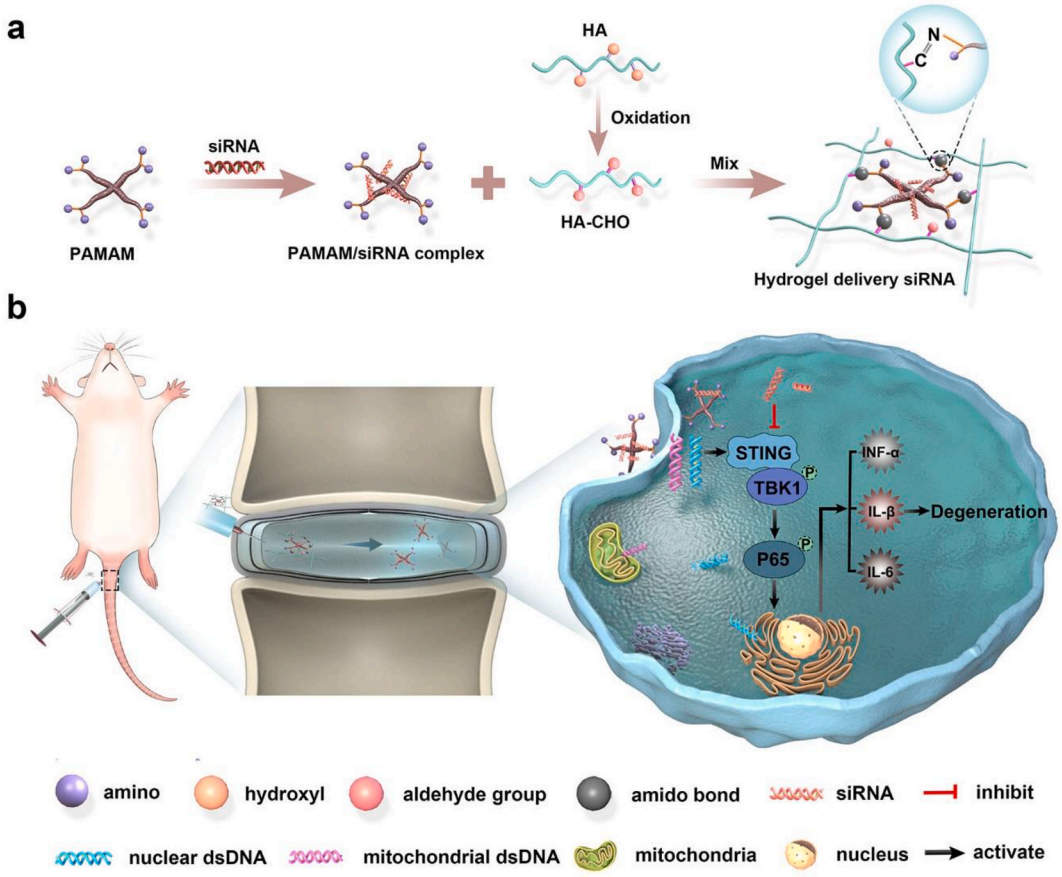

Scheme 1. Injectable self-healing hydrogel-based gene therapy of intervertebral disc degeneration. (a) The formation mechanism of the hydrogel with sustained siRNA releasing property. (b) The IVD degeneration therapy process using the as-fabricated hydrogel by sustained STING pathway silencing.

2.3. Synthesis of HA-CHO/PAMAM Hydrogel (HP^{gel}) or HA-CHO/PAMAM/siRNA Hydrogel (siRNA@HP^{gel})

Different concentration (*W/V*) of lyophilized HA-CHO and amine-terminated G5 PAMAM were dissolved in PBS respectively and then equal volume ratios were mixed by pipetting to form HP^{gel}. To obtain siRNA@HP^{gel}, PAMAM solution incubated with 2 μg siRNA for 10 min at room temperature to form PAMAM/siRNA polyplexes and then mix with equal volume ratios HA-CHO.

2.4. Characterizations of HP^{gel}

The HA-CHO and formation of hydrogel were verified *via* Fourier transform infrared spectroscopy (FT-IR, Vertex 70, Germany) and ^{1}H nuclear magnetic resonance spectroscopy (^{1}H NMR, AVANCE III 400 Hz, Switzerland). The internal microstructure of HP^{gel} was imaged with a field emission scanning electron microscope (Utral 55, Germany).

The gelation times were performed *via* a vial-tilting method [36]. 5% (W/V) HA-CHO in the presence of varying PAMAM concentrations (5%, 3%, 1%, 0.5% and 0.1% W/V) were put into 2 mL vials. The sol-gel transition time was determined by inverting the vial until the point at which no fluidity was observed. Each data point was derived from an average of three measurements. To determine the stability of the hydrogels, HP^{gel} was injected into the glass vial and incubated with PBS, then vials were placed at 37 °C for 24 h.

The injectability and self-healing performance macrographs of HP^{gel} were exhibited using a digital camera. A trace amount of dye that does not react with the hydrogel was added for better visualization. The hydrogels were extruded into PBS in glass vial through a 26-gauge needle and were also injected into "STING" shape. To study the self-healing nature, the hydrogel was sliced into two pieces, photos were captured at 0, 5, 10, and 15 min.

The dynamic rheological tests of HP^{gel} were conducted using a strain-controlled rheometer (Anton Paar MCR302, Austria). 1 mL of hydrogel was placed in a parallel plate (20 mm). Frequency sweep tests were performed between 0.1 and 10 Hz using a constant strain (1%) at 37 °C. A strain amplitude sweep test (γ = 1%–1000%) a constant angular frequency of 1 Hz at 37 °C was performed to obtain the critical strain point. For shear recovery experiments, the alternate strain sweep was tested, and the amplitude oscillatory strains were changed from small strain (γ = 1%) for 200 s to large strain (γ = 800%) for 50 s with 1 Hz frequency at 37 °C. The shear thinning experiments were characterized by measuring the linear viscosity with a shear rate range of 0.01–100 s^{-1} to at 37 °C.

Compression testing was carried out to evaluate the mechanical property by applying a strain rate of 1 mm/min using a dynamic mechanical analysis (DMA) (Q800, America). We determined the compressive modulus by taking the slope in the linear section of the stress-strain curve at 5%–10% strain area. Three replicates were used for each group.

To determine its swelling behavior, the freeze-dried hydrogel (W_0) was immersed in PBS and incubated at 37 °C. The wet mass (W_t) of the hydrogel was measured at various durations (0, 1, 2, 3, 4 and 6 h) and the swelling rate was calculated according to $((W_t\text{-}W_0)/W_0)$.

The degradation property of HP^{gel} was evaluated *in vitro* and *in vivo*. Briefly, the initial dry weight of the hydrogel was recorded and 400 μL of HP^{gel} was then submerged in 2 mL of PBS (pH = 7.4 and pH = 6.5) at 37 °C with shaking at 50 rpm. The residual weight of hydrogel was recorded at day 0.5, 1, 3, 5, 7, and 9. In addition, 1 mL of hydrogel was subcutaneously injected into the rat and photographed to record the *in vivo* degradation rate of the hydrogel at the 1st, 3rd, 7th, 14th and 21st

day.

2.5. siRNA encapsulation in HP^{gel}

Cy3 labeled siRNA was complexed with PAMAM and then mixed with equal volume HA-CHO to form hydrogel. The cy3-siRNA@HP^{gel} was then washed with PBS three times and observed using a confocal microscope (Nikon A1 Ti, Japan). In addition, agarose gel electrophoresis was also performed to evaluate the complex of siRNA/PAMAM and encapsulation of siRNA in hydrogel. Electrophoresis was carried out applying 1% (*W/V*) agarose gels containing ethidium bromide solution and samples consisting of 2 μg siRNA loaded in 50 μL of PBS, HA-CHO/PBS, PAMAM/PBS, and 50 μL HP^{gel} were loaded into each well of the gels. The gels were run for 20 min at 100 V and visualization of the siRNA bands was performed using an MF-ChemiBIS gel imaging system (DNR Bio Imaging Systems, Israel).

2.6. In vitro release of siRNA from siRNA@HP^{gel}

Cy3 fluorescently tagged siSTING was used to examine its release kinetics from HP^{gel}. 2 μg cy3-siSTING was complexed with 100 μL PAMAM to form polyplexes and then mixed with equal volume HA-CHO to form hydrogel. 200 μL cy3-siSTING@HP^{gel} were incubated with 500 μL PBS solution in 24 well plates at 37 °C in the dark and equal volume of cy3-siSTING@PAMAM/PBS solution (100 μL cy3-siSTING@PAMAM and 100 μL PBS) was used as control. At time points of 0, 0.125, 0.5, 1, 3, 5, 7 days, the supernatant was completely collected and replaced with fresh PBS solution. Release of siRNA was quantified fluorescently (545 nm/568 nm) using a plate reader (M200 PRO, Austria).

2.7. Release siRNA from HP^{gel} hydrogels in vivo

Cy5 labeled siSTING was used to examine its release from HP^{gel} *in vivo* and adult male Sprague-Dawley rats (aged 3 months, $n = 10$) were used for the experiments. Rats were randomly divided into two groups: 50 μL cy5-siRNA@HP^{gel} was injected into the rat Co6/7-disc space using 26-gauge needle and 50 μL cy3-siSTING@PAMAM/PBS solution was injected as control. Localization and release of cy5-siSTING (643/667 nm) were monitored via Caliper IVIS Lumina II (CLS136341/F, USA). IVIS was performed 0, 3, 7, 14, 21 days after injection using 1% isoflurane gas as anesthetic. Quantification of cy5-siRNA from IVIS imaging was achieved by measuring the total radiant efficiency and normalizing to day 0.

2.8. Rat IVD degeneration model

A total of 48 male Sprague-Dawley rats, aged 3 months, were used for the experiments *in vivo*. Forty rats underwent the surgery, and the remaining 8 rats underwent no surgical intervention as controls. The surgical procedure was described previously [37]. Briefly, rats were anesthetized with an intraperitoneal injection of pentobarbital sodium (45 mg/kg) and placed in a prone position. Then under fluoroscopic guidance, Co6/7 disc was punctured by a 20-gauge needle from the dorsal side. The needle punctured through the center of the disc until the opposite side, rotated 180°, and held for 10 s. The Co5/6 or Co7/8 disc is left intact as a self-control. One week after the initial puncture, the rats were randomly divided into 4 groups (noninjection, siSTING@HP^{gel}, siSTING@PAMAM, HA-CHO, and siSTING/PBS injection) with 8 rats in each group. After anesthesia, 50 μL materials was slowly injected into the Co6/7 disc using a 26-gauge needle. During the experiment process, there were no deaths or diseases. After four or eight weeks, the discs were harvested and investigated.

2.9. Statistical analysis

All data were expressed as means ± standard deviations (SDs). SPSS 20 software (IBM, USA) was used for statistical analysis. Kolmogorov–Smirnov test was used to assess the normality of parameters. Comparison of data between two groups was performed using a two-tailed Student's t-test. Multiple comparisons were assessed by one-way analysis of variance (ANOVA) with a post-hoc Tukey test. P values < 0.05 was considered a statistically significant difference.

2.10. Other methods

Methods that applied for human IVD harvest, qPCR, Western Blot, cell cultivation and treatment, cytosolic DNA extraction, *in vivo* radiography, MRI examination, and histological staining *etc*. are described in Experimental Section of Supporting Information.

3. Results and discussion

3.1. STING–NF–κB pathway activation and cytosolic DNA leakage in human degenerated NP tissues

It is well known that inflammatory responses of NP lead to ECM degradation and are considered a fairly important cause of IVD degeneration. Recently, a growing body of evidence has suggested that STING pathway plays a central role in inflammatory responses in numerous diseases such as chronic kidney disease [16], neurodegeneration [18], ischemic stroke [38]. To explore the role of STING in IVD inflammation, we firstly examined the expression of STING pathway and cytosolic DNA in human NP samples. The mRNA expression of STING in 28 IVD degenerated patients (Pfirrmann grade IV-V) and 16 controls (Pfirrmann grade I-II) was tested by qPCR, and it was significantly increased in the degenerated NP tissues (2.89-fold change). Then, three NP samples in each group were randomly selected for subsequent tests. IHC staining showed that the protein expression of STING was also upregulated in degenerated NP samples particularly in cell-clusters which was one of the histological characteristics of degenerated NP cells (Fig. 1a–c) [39].

Western blot analyses told the upregulated expression of STING, TBK1, p65 and phosphorylation TBK1, p65 in degenerated NP samples compared with controls (Fig. 1d), indicating that the STING–NF–κB pathway was activated in degenerated NP tissues. Moreover, coimmunostaining of double-stranded DNA (dsDNA) and the mitochondrial marker Tomm20 was used to test the cytosolic DNA that did not colocalize in nucleus or mitochondria. Immunofluorescence staining results showed that compared with control tissues, degenerated NP had a markedly increased amount of cytosolic DNA in cells (Fig. 1e–**f**), which hinted DNA damage and leak of DNA to the cytosol in degenerated tissues. Together, these results demonstrated that STING pathway activation and cytosolic DNA leakage were associated with IVD degeneration.

3.2. H_2O_2-induced STING –NF–κB pathway activation by the leakage of cytosolic DNA

We further examined the function of STING on human NP cells *in vitro*. ROS play a crucial role in the pathogenesis of IVD degeneration that have been proved by our and many other previously studies [40–42]. Hence, H_2O_2 was used to induce inflammation and degeneration in NP cells *in vitro*. Firstly, we assessed whether STING–NF–κB pathway would response to ROS stimulation, and NP cells were treated with different concentrations of H_2O_2 for 2 h. Interestingly, the STING–NF–κB pathway could be activated dose-dependently with H_2O_2 stimulation evidenced by the increased levels of STING, phosphorylation of TBK1, and p65 proteins (Fig. 2a). Moreover, pretreatment with N-acetylcysteine (NAC), a widely used antioxidant, can observably inhibited STING signaling activation even induced by 500 μM H_2O_2 (Fig. 2b), indicating that ROS can truly promote the expression of STING–NF–κB pathway in NP cells. Consisting with our findings, ROS was once proved to potentiate STING-dependent type I IFN induction in

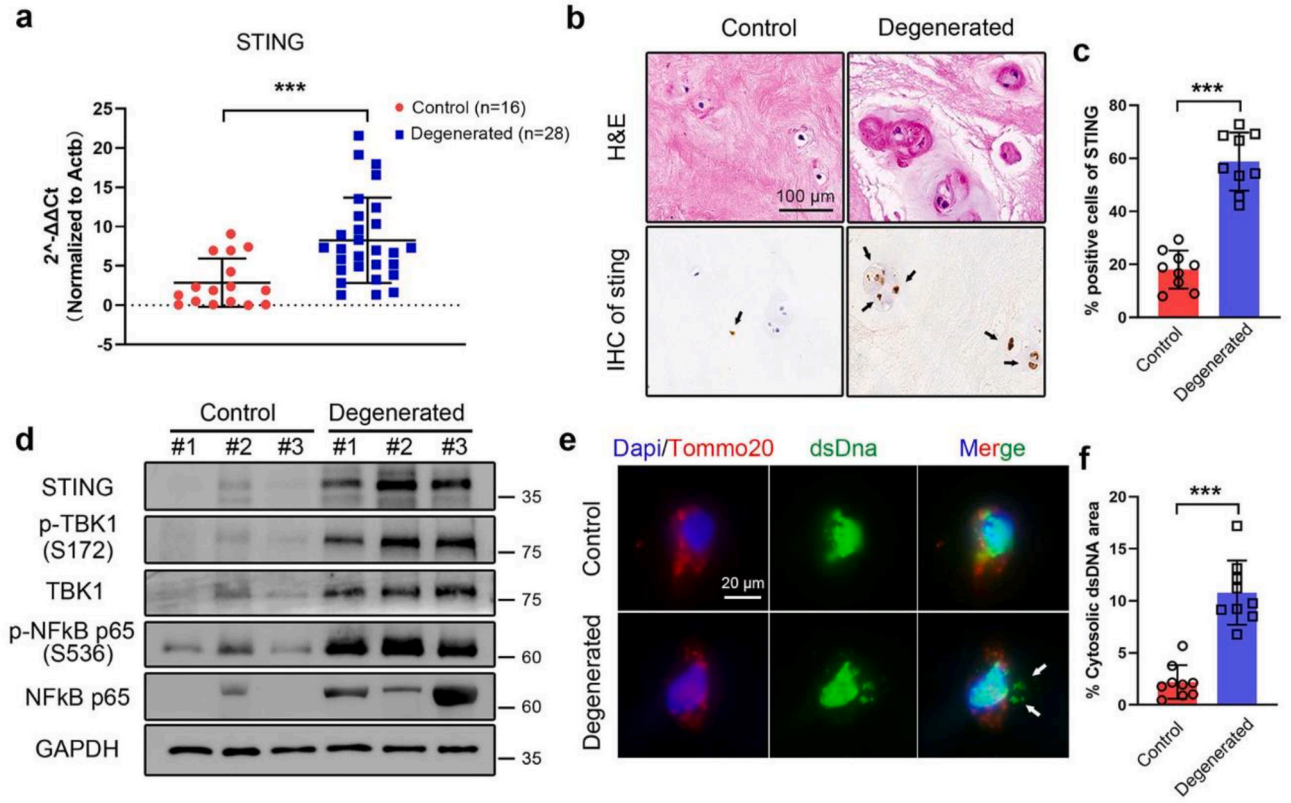

Fig. 1. STING–NF–κB pathway activation and cytosolic DNA leakage in human degenerated NP tissues. (**a**) mRNA expression of STING by qPCR analysis in the degenerated NP tissues ($n = 28$ patients) compared with controls ($n = 16$ patients). (**b**) Representative HE and STING immunohistochemistry (IHC) staining images in human NP tissues. Positive cells were marked with black arrows. (**c**) Quantification positive cells of STING in IHC images by Image J ($n = 3$ patients with three independent sections in each group). (**d**) Representative western blots of STING–NF–κB pathway expression in the degenerated NP tissues compared with controls from three independent experiments ($n = 3$ patients in each group). (**e**) Representative immunofluorescence staining of dsDNA (green) and mitochondria (Tomm20, red) in human NP tissues. Nuclei were counterstained with DAPI (blue). Cytosolic dsDNA that did not colocalize in nucleus or mitochondria was indicated with white arrows. (**f**) Quantification cytosolic dsDNA area normalized to total dsDNA area in IF images analyzed by Image J ($n = 3$ patients with three independent sections). The values presented are the means ± SDs. $^{***}P < 0.001$. Statistical significance was determined using a two-tailed Student's t-test. (For interpretation of the references to color in this figure legend, the reader is referred to the Web version of this article.)

dendritic cells [43] and Luo et al. reported that ROS activated the STING pathway in Aortic smooth muscle cells [17]. However, cellular oxidative stress by reported can prevent the activation of STING-dependent DNA sensing in macrophages during DNA viral infection in mechanism that oxidized cysteine 178 or 179 on STING induced by ROS [44]. These seemingly opposing results are likely due to the different cell types utilized.

STING has currently been defined as a key cytosolic DNA sensor and cytosolic dsDNA is recognized by STING, stimulating inflammatory cytokine generation (*e.g.,* TNF-α and IL-1β) *via* NF-κB pathway [16]. Next, we tested whether ROS could induce accumulation of DNA in the cytosol thus activating STING–NF–κB pathway. Confocal analysis showed that treating NP cells with H_2O_2 markedly increased the accumulation of dsDNA outside nuclei, and mitochondria as well (Fig. 2c–d). The quantification of DNA in the cytosolic fraction showed a significant increase in the amount of cytosolic dsDNA in H_2O_2 treated NP cells (Fig. 2e). Again, the dramatic increase in DNA within the cytosolic fraction in H_2O_2 treated NP cells was proved by agarose gel analysis, and the fragment size of DNA is around 100 bp (Fig. 2f). To examine whether H_2O_2 stimulation can result in mtDNA release into the cytosol, we quantified the mtDNA amount using qPCR (Fig. 2g). It was found that significant enrichment for mtDNA, such as mt-Co1, mt-Rnr2, and mt-Nd6 in the cytosolic compartments of H_2O_2 treated NP cells as compared to control cells. These data supported the possibility conclusion that ROS caused DNA damage and release of DNA fragments into the cytosol in NP cells *in vitro,* which was quite consistent with our previous results that accumulation of cytosolic DNA in degenerative NP specimens elevated oxidative stress levels in degenerative IVD specimens [41].

3.3. *STING inhibition can reduce inflammation and degeneration induced by H_2O_2 in NP cells*

To further examine the feasibility of targeting STING in inflammation and degeneration in NP cells induced by H_2O_2 for IVD degeneration therapy. The expression of STING in NP cells was knocked down by STING siRNA with commercial Lipofectamine 3000 transfection. As shown in Fig. 3a–c, STING silencing significantly inhibited ROS-induced TNF-α, IL-1β, IL-6 mRNA expression in NP cells. Additionally, Western blot analysis (Fig. 3d) uncovered that ROS downregulated the protein expression levels of primary constituents in ECM including collagen II and aggrecan, at the meantime upregulated the major catabolic factors such as Mmp3 and Mmp13, while knock-down of STING significantly reversed these effects. These results demonstrated that STING inhibition significantly reduced production of proinflammatory cytokines caused by ROS, leading to a homeostatic balance between anabolism and catabolism thus suppressing degeneration of NP cells [37].

It has been reported that NF-κB pathway is involved in mediating inflammatory in the IVD [45], and it is one of downstream pathways dependent to STING [21]. As shown in Fig. 3e, STING silencing reduced the phosphorylation level of TBK1 and p65 in the presence of H_2O_2 as

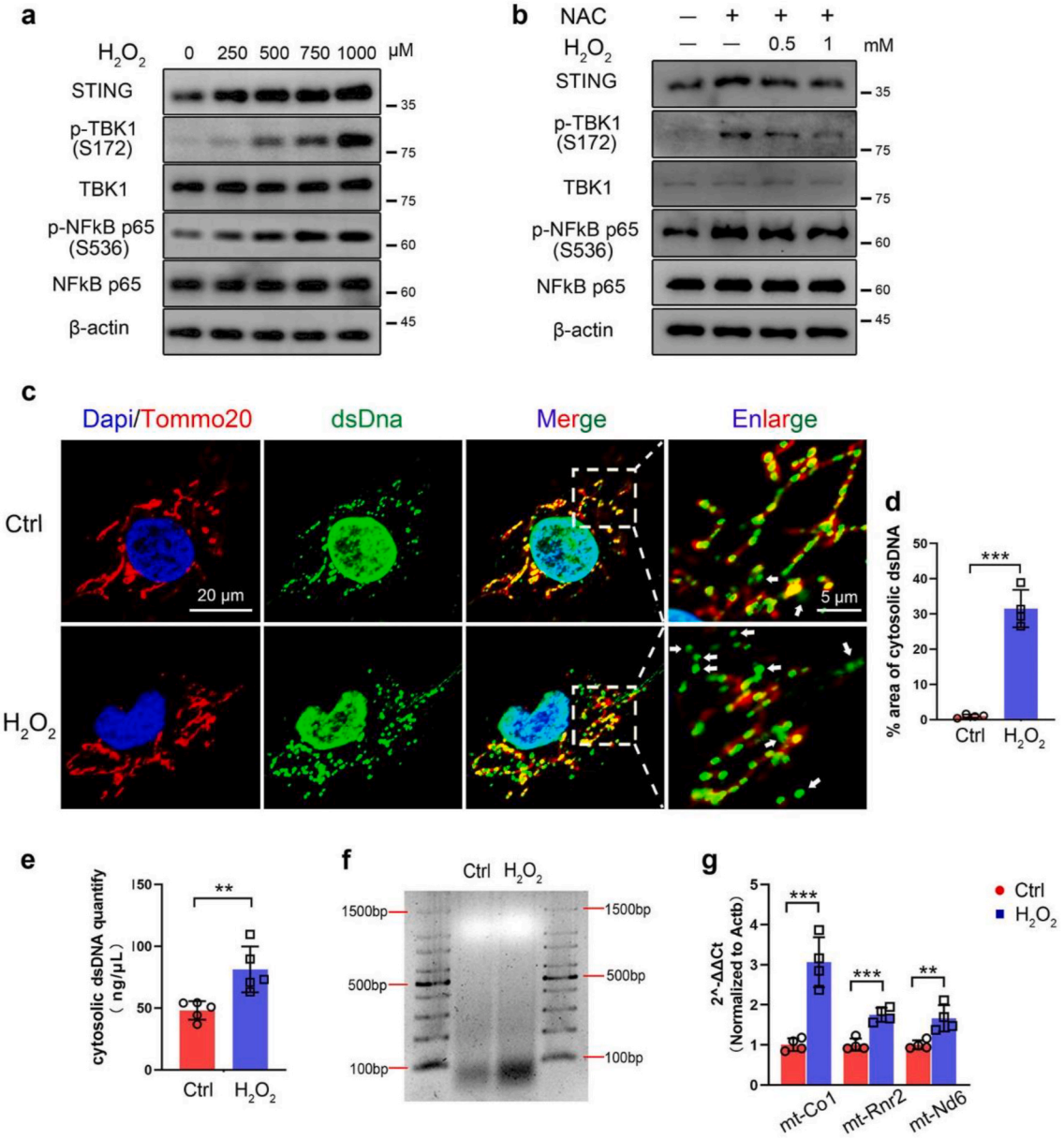

Fig. 2. H_2O_2-induced STING–NF–κB pathway activation by the leakage of cytosolic dsDNA. (**a**) Representative Western blot analysis of STING–NF–κB pathway expression in NP cells treated with 0, 250, 500, 750, 1000 μM H_2O_2 for 2 h. Representative images are shown from three independent experiments. (**b**) Representative Western blot analysis of STING–NF–κB pathway expression in NP cells pre-exposed 0.5 mM NAC (N-acetylcysteine) for 1 h followed by 500 μM H_2O_2 treatment for 2 h. Representative images are shown from three independent experiments. (**c**–**g**) NP cells were treated with 500 μM H_2O_2 for 2 h for subsequent analysis. (**c**) Representative confocal analysis of IF staining of dsDNA (green), mitochondria (Tomm20, red), and nuclei (DAPI, blue) in treated NP cells. Cytosolic dsDNA that did not colocalize in nucleus or mitochondria was indicated with white arrows. (**d**) Quantification cytosolic dsDNA area normalized to mitochondrial dsDNA area in IF images analyzed by Image J ($n = 4$ independent experiments). (**e**) Quantitative detection of dsDNA (ng/μL) in the cytosolic fraction of H_2O_2 treated NP cells or controls ($n = 5$ independent experiments). (**f**) Representative agarose gel images of dsDNA in the cytosolic fraction in treated NP cells. (**g**) mRNA expression of mtDNA including mt-Co1, mt-Rnr2, and mt-Nd6 by qPCR analysis in treated NP cells ($n = 4$ independent experiments). The values presented are the means ± SDs. $^{**}P < 0.01$; $^{***}P < 0.001$. Statistical significance was determined by a two-tailed Student's t-test for **d**, **e** and by one-way ANOVA with a post-hoc Tukey test for **g**. (For interpretation of the references to color in this figure legend, the reader is referred to the Web version of this article.)

analyzed by Western blot. Furthermore, immunofluorescence staining showed a decreased nuclear translocation of the p65 subunit of NF-κB by STING knockdown (Fig. 3f–**g**), indicating that STING activation led to NF-κB pathway activation of NP cells in coincide with some other cellular systems [16,46]. The STING knockdown in cultivated NP cells without H_2O_2 stimulation slightly reduced mRNA expression of IL-1β and regulated ECM constitutions, which might be ascribed to the NF-κB inhibition. Conclusively, ROS promoted the release of mtDNA and nuclear DNA into the cytosol, and initiated inflammatory responses by activating the STING–NF–κB pathway, revealing a novel pathway and mechanism regulated by ROS in IVD degeneration. Moreover, accumulating evidence indicates that DNA damage riggers inflammatory response and cellular senescence in NP cells [23,47]. Herein, our study provided a new sight for linking DNA damage in degenerated IVD to a cytosolic DNA sensing STING and indicated STING may be a potential therapeutic target for IVD degeneration. Interestingly, a very recently study by Guo et al. shown that STING promote apoptosis, senescence and ECM degradation of NP cells induced by oxidative stress through activating IRF3 pathway which also confirmed our results and strongly hinted STING as a target for the treatment of IVD degeneration.

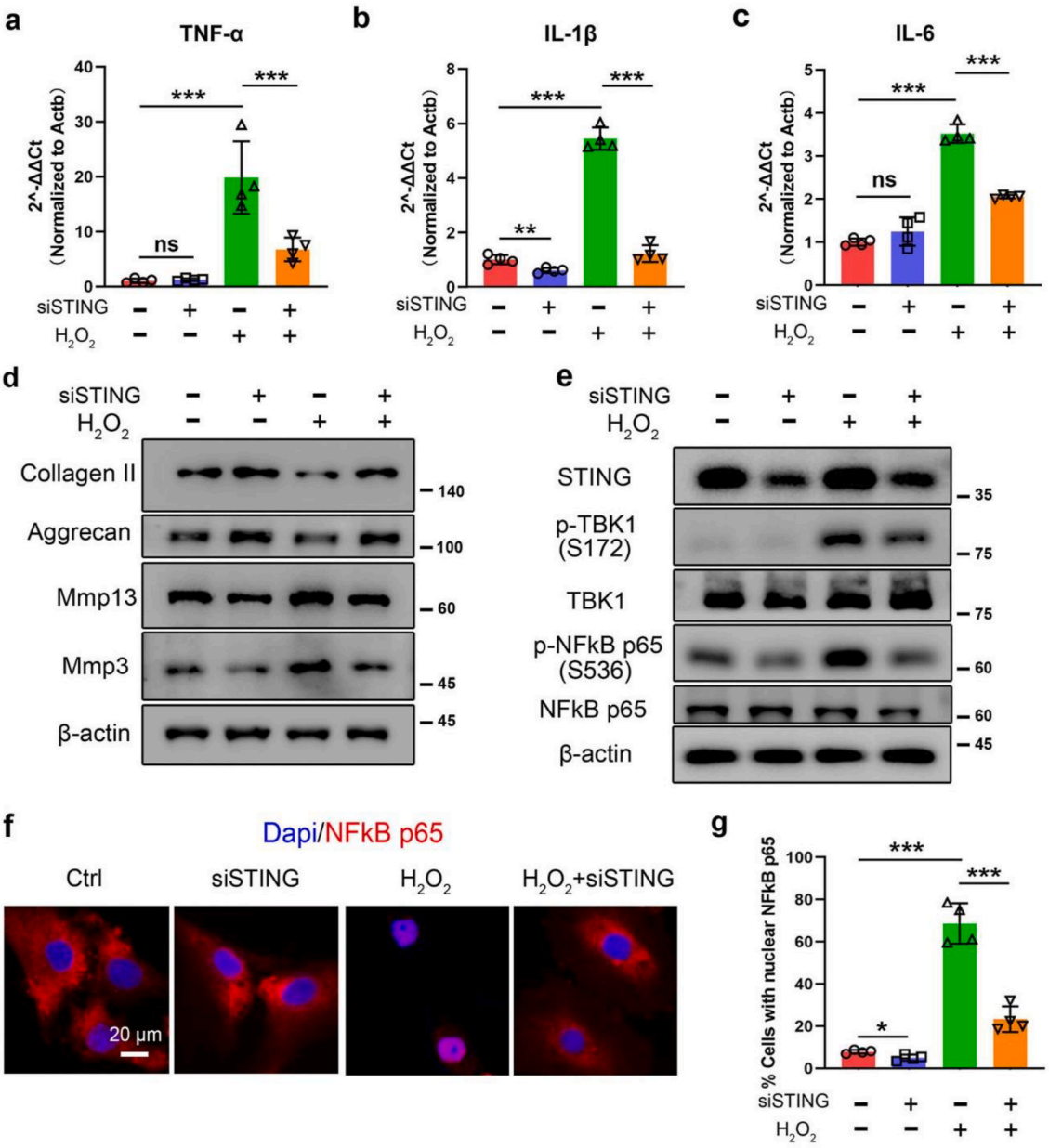

Fig. 3. STING inhibition reduced inflammatory and degenerative phenotypes of NP cells induced by H_2O_2. (**a**–**d**) NP cells were pre-exposed to negative control siRNA or siSTING followed by 500 μM H_2O_2 treatment for 48 h. The relative mRNA amount of TNF-α (**a**), IL-1β (**b**), IL-6 (**c**) was determined by qPCR ($n = 4$ independent experiments). (**d**) Representative Western blot images of collagen II, aggrecan, Mmp3, Mmp13 protein expression in treated NP cells from three independent experiments. (**e**–**g**) NP cells were pre-exposed to negative control siRNA or siSTING followed by 500 μM H_2O_2 treatment for 2 h. (**e**) Representative Western blot images of STING–NF–κB pathway expression in treated NP cells from three independent experiments. (**f**) Representative IF staining of p65 in treated NP cells. (**g**) Quantitative analysis of cells with nuclear p65 in IF images ($n = 4$ independent experiments). The values presented are the means ± SDs. $^*P < 0.05$; $^{**}P < 0.01$; $^{***}P < 0.001$; ns, not statistically significant. Statistical significance was assessed by one-way ANOVA with a post-hoc Tukey test.

3.4. Design, synthesis, and characterization of hydrogels for siRNA delivery

In our study, we have proved that STING represents an attractive target for therapeutic intervention in IVD. At present, a few specific small molecule inhibitors of STING such as C-176, H-151 have been developed to treat STING-related diseases [48,49]. However, small molecule inhibitors are often associated with high toxicity and premature degradation. Short interfering RNA (siRNA) is a powerful gene silencing tool which inhibits gene expression at the post-transcriptional level. Application of siRNA provides an ideal potential therapy in many diseases for its merits of specificity to target mRNA and acting on any proteins [24,25]. However, there is currently a paucity of reports on siRNA-based therapy for IVD degeneration and a suitable vector is needed to be developed to conquer shortcomings of siRNA such as low cellular uptake, short half-life, and fast clearance. In the repair of IVD degeneration, one of the current focuses is on developing injectable *in situ* forming hydrogels to deliver bioactive agents or cells in a sustained and minimally invasive manner [8]. Importantly, it has been reported that hydrogel systems can achieve sustained and long-term delivery of siRNA [50]. Therefore, a novel hydrogel that delivers siRNA of STING is aiming to be designed to treat IVD degeneration.

The hydrogel for siRNA delivery was prepared by formation of dynamic Schiff base bonds between HA-CHO and multiple amino-terminal PAMAM (Fig. 4a). The aldehyde groups were introduced on the surface of HA *via* periodate oxidation as reported in the literature [35]. The

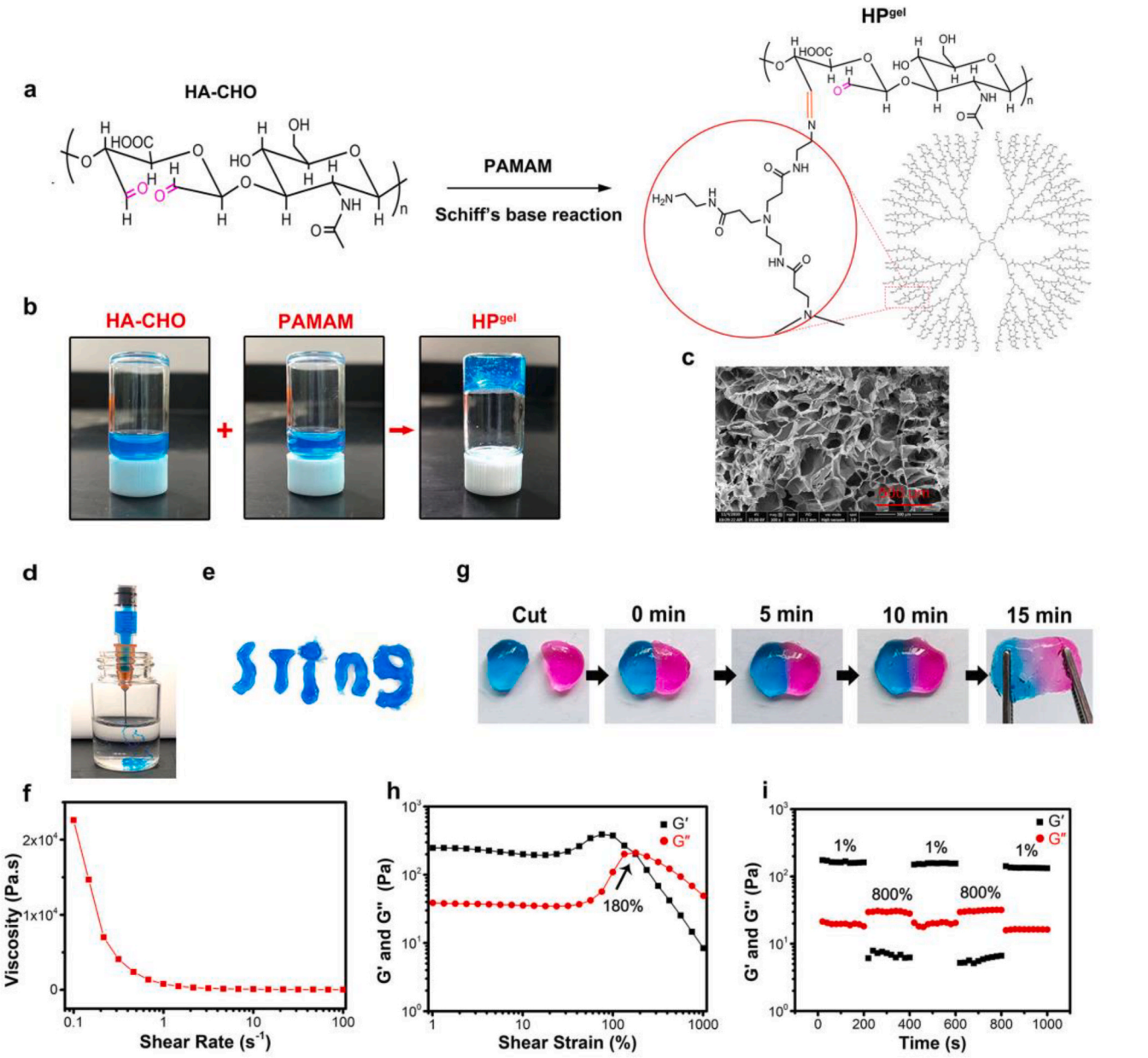

Fig. 4. Preparation of the HP^{gel} hydrogel and injectability, self-healing properties of the hydrogel. (**a**) Scheme of the prepared HP^{gel} hydrogel by formation of Schiff base bond. (**b**) Photographs of HP^{gel} hydrogel formation. (**c**) SEM images of the hydrogel. (**d**) Image of HP^{gel} injected from a 26-gauge needle into PBS. (**e**) Photographic images of HP^{gel} injected into "STING" shape. (**f**) Viscosity with increasing shear rates (0.1–100 s^{-1}) showing shear-thinning feature of the hydrogel. (**g**) Photographs of the macroscopic self-healing capacities of the hydrogel. Two pieces of cut HP^{gel} hydrogel artificially stained by rhodamine B and methylene blue, respectively, and healed after being kept in contact for 15 min. (**h**) G′ and G″ of the hydrogel in the strain amplitude sweep (g = 1%–1000%) at a fixed frequency (1 Hz). (**i**) Rheological behaviors of the hydrogel with alternate strains switched from 1% to 800%. (For interpretation of the references to color in this figure legend, the reader is referred to the Web version of this article.)

adjacent hydroxyls on the HA backbone were partially oxidized to form aldehyde groups by employing sodium periodate as the oxidizing agent. The oxidation degree of HA was about 51.6% as confirmed by a hydroxylamine hydrochloride assay (Table S1). The HA aldehyde was further identified by ^{1}H NMR spectroscopy, in which the new peaks at 5.0 ppm and 5.1 ppm corresponded to protons from the aldehyde group and adjacent hydroxyls (Fig. S1) [51].

To optimize the composition of hydrogel for gel-formation, the gelation time was determined by equal volume mixture of varying concentration of PAMAM (wt%) and 5% (wt%) HA-CHO. Gelation time was prolonged by a reduced concentration of PAMAM (Fig. S2) possibly for decreased density of the cross-linked network. As is known, PAMAM dendrimers are excellent candidates for delivery drugs or genes due to good special three-dimensional structure, biocompatibility, multivalent surface, and internal cavities [52]. Moreover, G5 PAMAM as cationic dendrimers have been shown to mediate efficient cellular uptake and transfection of siRNA in multiple studies [53]. However, in consideration of possible cytotoxicity associated with dendrimers [54] and based on results of the gelation time, we used 1% (wt%) PAMAM in further investigations. Furthermore, Fig. S3 showed that the storage modulus tested by rheological measurement and compressive modulus calculated from strain-stress curves increased with increasing HA-CHO concentration at the fixed PAMAM amount, which reflected the strengthened mechanical properties of hydrogels. In our study, we chose 5% (wt%) HA-CHO and 1% (wt%) PAMAM for the subsequent experiment.

As shown in Fig. 4b, the mixture of equal volume HA-CHO and

PAMAM solution could form hydrogel (HP^{gel}) rapidly (within 30 s) at room temperature. Moreover, there was no obvious dissolution of HP^{gel} after incubation in PBS at 37 °C for 24 h, demonstrating a good stability of hydrogel structure under physiological conditions (Fig. S4). And the swelling equilibria of HP^{gel} reached 2196% ± 159% after immersing in PBS for 4 h (Fig. S5). Scanning electron microscopy (SEM) of lyophilized HP^{gel} showed a typical porous microstructure of hydrogels (Fig. 4c). FT-IR was used to further confirm the formation of hydrogel (Fig. S6). A new infrared peak at 1722 cm^{-1} in HA-CHO was ascribed to the C═O stretch, confirming the presence of aldehyde groups compared to HA [51]. And the peak around 1548 cm^{-1} characterized the primary amino group (-NH_2) at PAMAM, whose intensity decreased in the spectrum of HP^{gel}, indicating the consumption of –NH_2 during the reaction to form Schiff base bonds.

Injectable hydrogels designed for minimally invasive treatment and self-healing hydrogels with rapid shape-recovery ability, making the hydrogels resistant to broken and leakage that were important for *in vivo* applications [34]. Therefore, the injectability and self-healing properties of HP^{gel} were evaluated. The hydrogels were extruded into PBS through a 26-gauge needle and could be continuously injected to draw the letter "STING" without clogging (Fig. 4e). Meanwhile, the viscosity of hydrogel dramatically decreased when the shear rate increased from 0.1 to 100 s^{-1}, demonstrating the shear-thinning and injectable capacity of the gel (Fig. 4f). Next, the self-healing behavior of the hydrogel was conducted by a macroscopic test and rheological recovery test. As showed in Fig. 4g, two separated hydrogels could form a single and complete hydrogel within 15 min after being put together.

The strain sweep of the hydrogel showed that G′ (storage modulus) and G″ (loss modulus) of the hydrogel remained almost constant until the strain reaches around 100% (Fig. 4h), suggesting that the hydrogel can sustain relatively large elastic deformations. However, the G′ and G″ intersected at a point of 180%, which was the critical point indicating that the collapse of the hydrogel network occurred. Subsequently, a continuous alternative strain sweep was conducted to determine the autonomous healing behavior of the hydrogel (Fig. 4i). When a high dynamic strain (800%) was applied, the value of G′ was dropped and lower than that of G″, demonstrating the damage of the gel network. Once the strain was switched to a low value (1%), the hydrogel showed complete recovery of G′ and G″ within seconds even after three alternately repeating cycles, indicating an excellent self-healing ability. Dynamic Schiff base reaction has been introduced in hydrogels and occurs at room or physiological temperature rapidly. The reaction of aldehyde groups in HA-CHO and amino groups in PAMAM forming Schiff base bonds allowed a dynamic equilibrium and endowed the hydrogel injectability and self-healing properties [35].

Next, the degradation properties of the hydrogel *in vitro* and *in vivo* were evaluated. As shown in Fig. S7a, the hydrogel degraded over time and completely biodegradable within 9 days in an equilibrium solution (PBS) with oscillation. Due to the acid-sensitive character of the Schiff base bond, degradation behavior of the hydrogel was also tested in pH 6.5 PBS according to previous studies, where pH 6.5 medium was used to simulate acidic stress as a result of the local overactive inflammatory response in the IVD [55,56]. 400 μL of HP^{gel} was almost fully degraded within 7 days in solution of pH 6.5, verifying a representative pH-responsive degradation property *in vitro*. Furthermore, the hydrogel injected subcutaneously of the rat back was also mostly degraded within 14 days *in vivo* (Fig. S7b), and no obvious residue could be seen at day 21. These results indicated an outstanding pH-responsive degradation and biodegradable properties of the hydrogel.

We hypothesized those electrostatic interactions between siRNA and PAMAM formulated siRNA polyplexes. Subsequently, hydrogel can be fabricate using the formation of Schiff base bonds between HA-CHO and PAMAM to encapsulate the siRNA, and the siRNA polyplexes can dissociate from the hydrogel over time, which could transfect into cells. The cationic polymers PAMAM acted as both the efficient transfection reagent and network component. The free siRNA was visualized using gel electrophoresis. Fig. S8 told that the siRNA was full complexed with PAMAM and encapsulated in the hydrogel as compared to free siRNA, siRNA/HA-CHO mixture, indicated by a strong RNA band in control siRNA, siRNA/HA-CHO lines, and no siRNA band in siRNA/PAMAM, siRNA@HP^{gel} lines. Moreover, fluorescence observation directly showed that cy3-labled siRNA was dispersed in the HP^{gel} (Fig. S9). Next, cy3-labeled siRNA was assembled with PAMAM and then incorporated into HP^{gel} and the siRNA release property *in vitro* was measured (Fig. S10). The siRNA percentages released were 22.63 ± 4.08, 48.40 ± 6.55 and 80.03 ± 3.78 over 1, 3 and 5 days, respectively. These results indicated that siRNA complexes were retained in the hydrogels and can be slowly released over a prolonged period of time *in vitro*. The sustained release observed was most likely due to the electrostatic interactions between PAMAM and the anionic phosphates of the siRNA as well as being encapsulated within the hydrogel structure, thus limiting diffusion of siRNA. Taken together, these results confirm that the hydrogel of HP^{gel} possesses rapid gelation time, excellent injectability, efficient self-healing ability, and prolonged siRNA released characteristic which may be favorable for treating IVD degeneration.

3.5. HP^{gel} mediated efficient, sustained siRNA uptake and STING silence in NP cells and prolonged release siRNA in vivo

Biocompatibility is of crucial importance for materials applied in the biomedical field [57]. The cytotoxicity of the HP^{gel} was next evaluated to determine its biocompatibility. The cytotoxicity was initially evaluated *via* CCK-8 assay by *co*-culturing with different contents of PAMAM, HA-CHO, and HP^{gel} with human NP cells. As shown in Fig. S11a, the viability of NP cells treated with different contents of PAMAM, HA-CHO, and HP^{gel} maintained about 100% viability after 1, 3, 5 days of incubation. To further evaluate the biocompatibility of the HP^{gel}, live/dead cell viability assays were performed. As shown in Fig. S11b, almost no dead cells were observed following *co*-cultured with HP^{gel} and cell proliferation occurred after 1, 3, 5 days of incubation, indicating that the hydrogel was non-toxic and of good cytocompatibility.

After this, to confirm the hydrogel system is capable of robust, sustained siRNA-mediated gene regulation, cellular uptake of siRNA in NP cells *in vitro* was firstly investigated by fluorescent imaging after co-culturing with cy3-siSTING@Lipofectamine 3000, cy3-siSTING@PAMAM, cy3-siSTING@HP^{gel} for 1, 3, 5 days. As showed in Fig. 5b−**e**, the maximal cellular uptake through lipofectamine 3000 and PAMAM was achieved at 1 days after transfection and then the cellular uptake percent gradually decreased. Meanwhile, the cellular uptake through PAMAM was higher than that of lipofectamine 3000 transfected, but the cellular uptake in NP cells by HP^{gel} system exhibited significantly increase at day 3 compared with day 1 and still maintained high cellular uptake percentage in day 5, indicating PAMAM mediated efficient transfection of siRNA and HP^{gel} system achieved sustained release. To prove that the hydrogels can preserve the bioactivity of siRNA over the release period, protein expression of STING was tested by Western blot. siSTING@Lipofectamine 3000 and siSTING@PAMAM provided transient STING knockdown at day 1 and 3 (Fig. 5f).

At day 5, STING expression partially recovered compared with control group. For NP cells treated with siSTING@HP^{gel}, the sustained knockdown of STING was observed, and the expression was lower at day 5 than day 1 & 3. These results demonstrated that sustainedly released siRNA from HP^{gel} were able to enter cells through endocytosis and escape the endosome to permit robust gene silencing. Then injection of cy5-siRNA@HP^{gel} and siRNA@PAMAM into rat discs respectively was to study the release behavior of siRNA *in vivo* (Fig. 6a). As showed in Fig. 6b−c, injection of siRNA@PAMAM showed rapid dispersal and clearance from disc site by day 7 with a $t_{1/2}$ of 1.9 days. Like the *in vitro* data, siSTING from the hydrogel persisted at the disc site for continue 21 days with $t_{1/2}$ of 6.3 days. While *in vivo* release time was longer than *in vitro* release, due to a relatively closed disc space which limited siRNA rapid diffusion [29]. The results indicated that HP^{gel} was able to

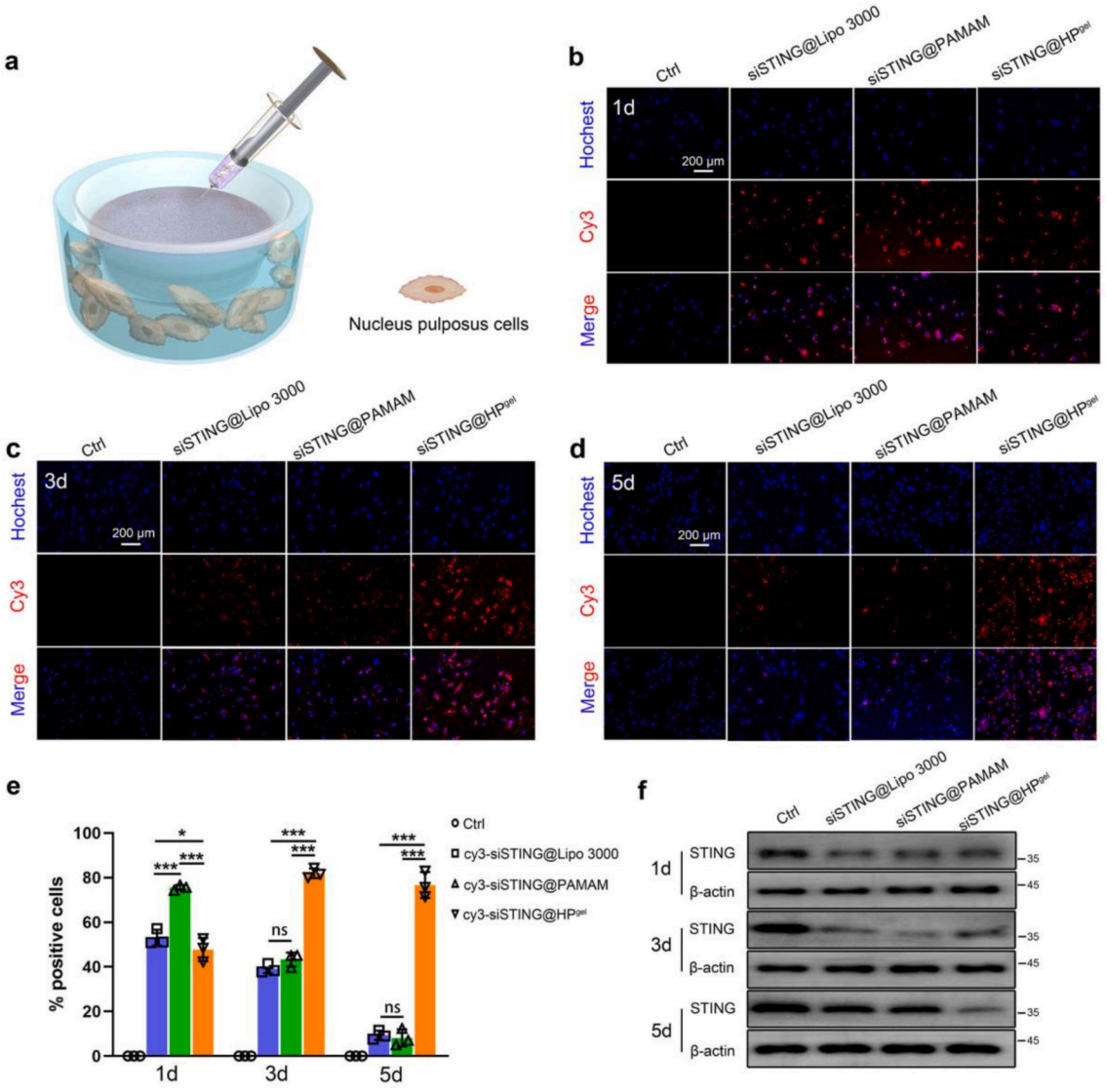

Fig. 5. siSTING@HP^{gel} mediated robust, prolonged cellular uptake and STING silencing in NP cells *in vitro*. (**a**) Schematic illustration of human NP cells *co*-cultured with hydrogel. Different experimental components were injected to cell culture inserts (3 μm pore size) and NP cells were seeded at the bottom. (**b**–**d**) Representative fluorescence images of the intracellular uptake of siRNA after *co*-culturing 1, 3, 5 days with PBS, cy3-siSTING @Lipofectamine 3000, cy3-siSTING@PAMAM and cy3-siSTING@HP^{gel} groups. Blue for nucleus (Hoechst) and red for cy3-labled. (**e**) Quantitative analysis of positive cells in fluorescence images ($n = 3$). (**f**) Representative Western blot of expression of STING in above-mentioned treated NP cells from three independent experiments. The values presented are the means ± SDs. $^{*}P < 0.05$; $^{***}P < 0.001$; ns, not statistically significant. Statistical significance was assessed by one-way ANOVA with a post-hoc Tukey test. (For interpretation of the references to color in this figure legend, the reader is referred to the Web version of this article.)

maintain high local concentration of siRNA in the surrounding tissues over an extended period.

3.6. Therapeutic efficacy of siSTING@HP^{gel} in puncture-induced rat IVD degeneration model and sustained STING knockdown in vivo

The therapeutic effects of siSTING@HP^{gel} were next evaluated using the puncture-induced rat IVD degeneration models (Fig. 7a) as described elsewhere [34,37]. Discs of rats were injected with siSTING@HP^{gel}, siSTING@PAMAM, HA-CHO or siSTING with a 26G needle while the control group received no needle puncture and the injured group received no injection. Radiographic assessment of disc height index (DHI) across the six groups revealed that at postoperative week 4, the DHI values in siSTING@HP^{gel} group were similar to those in the control group, but were significantly greater than those in siSTING@PAMAM, HA-CHO, siSTING and non-injection group. While slightly higher DHI values in siSTING@PAMAM and HA-CHO group compared with the siSTING and non-injection group were observed. Further, siSTING@HP^{gel} group demonstrated greater DHI than other puncture groups, while there was no significant difference between siSTING@PAMAM, HA-CHO, siSTING and non-

Injection group at 8 weeks postoperatively (Fig. 7b−**c**). The results indicated that siSTING@HP^{gel} could significantly delay puncture-induced disc height reduction while single siSTING@PAMAM, HA-CHO or siSTING had little therapeutic effects. MRI analysis can reflect the water content of IVD and is a crucial metric for IVD degeneration diagnose [58]. As shown in Fig. 7d−e, the trend of MRI analysis results were similar to radiographic assessment. Both the DHI values and MRI assessment were consistent and suggested the potential of siSTING@HP^{gel} system *in vivo*.

The minimally invasive injection of siSTING@HP^{gel} and the prolonged silence of STING, restrained IVD inflammation and degeneration process, as confirmed by the IVD tissue analysis by histology and immunohistochemistry at 4- and 8-week points. Hematoxylin and eosin

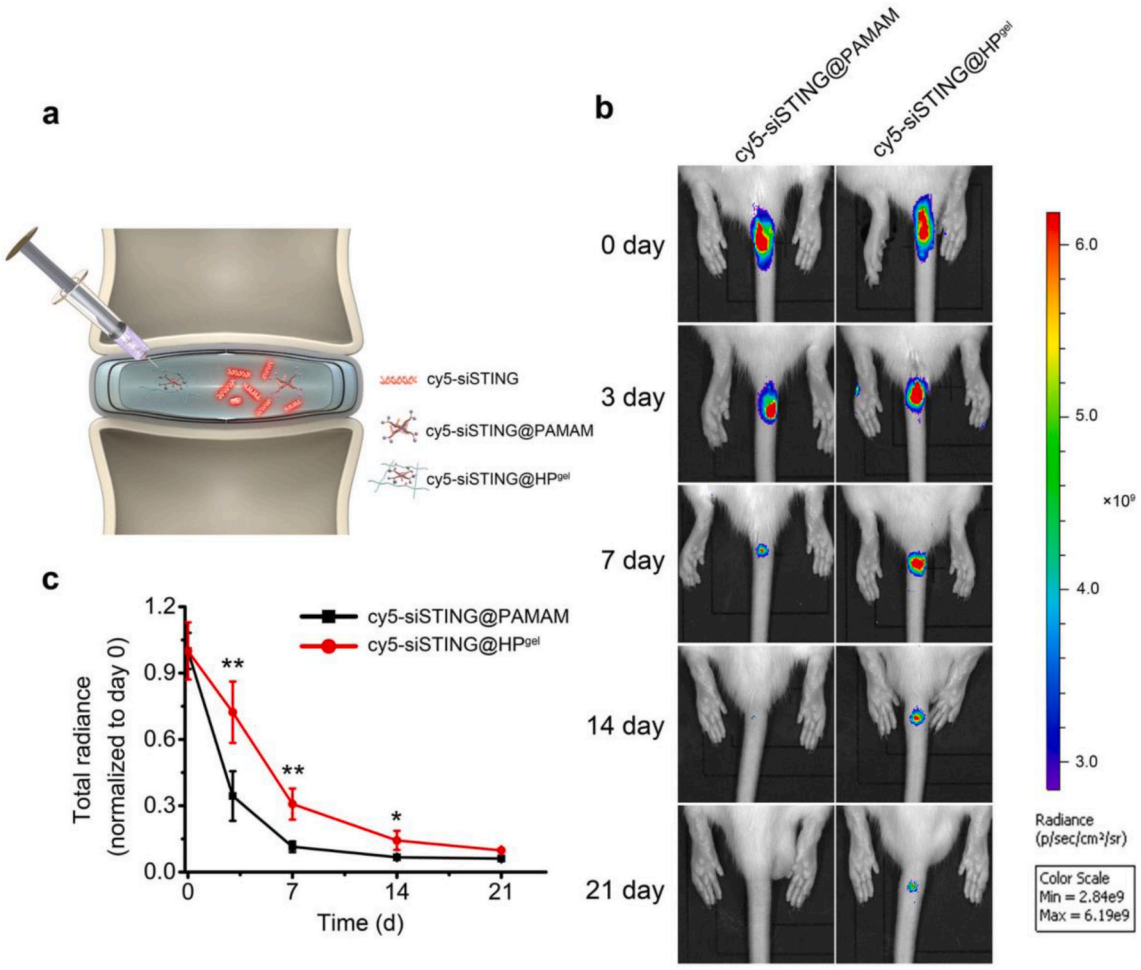

Fig. 6. Prolonged *in vivo* release of siRNA by siSTING@HP^{gel} at disc site. (**a**) Schematic illustration of injection cy5-siSTING@PAMAM and cy5-siSTING@HP^{gel} into disc space. (**b**) Representative IVIS images at rat disc site over time. The color bar (from blue to red) indicates the change in fluorescence signal intensity from low to high. (**c**) Quantification of cy5-siSTING from IVIS imaging. Data showed the total radiant efficiency of drawn region of interest in IVIS images normalized to day 0 (n = 5 individual rats in each group). The values presented are the means ± SDs. *P < 0.05; **P < 0.01. Statistical significance was determined using a two-tailed Student's t-test. (For interpretation of the references to color in this figure legend, the reader is referred to the Web version of this article.)

(H&E) staining was used to survey the NP morphology, fibrous tissue, and their margins [34]. From 4 to 8 weeks, a decreased NP tissue area was observed in siSTING@HP^{gel} group, but the loss was significantly lower compared with siSTING@PAMAM, HA-CHO, siSTING non-injection groups. In addition, blurred boundary between NP, annulus fibrosus, and sharply atrophied NP area were noted in the siSTING@PAMAM, HA-CHO, siSTING, and non-injection groups. Safranin O and Fast Green staining was used to the content of proteoglycans in NP. In the control group, the NP area was filled with proteoglycans, while the siSTING@PAMAM, HA-CHO, siSTING and non-injection groups demonstrated significantly reduced proteoglycans levels. And the loss of proteoglycans in siSTING@HP^{gel} group was lower than other puncture groups (Fig. 7f). The histological grade indicated that the siSTING@HP^{gel} (4.75 ± 0.50; 7.00 ± 0.82) treatment were much lower than siSTING@PAMAM (9.00 ± 0.82; 11.50 ± 0.58), HA-CHO (8.00 ± 0.82; 11.25 ± 0.96), siSTING (11.00 ± 0.82; 11.50 ± 0.57) and non-injection (11.50 ± 0.58; 11.75 ± 0.50) groups at 4 and 8 weeks, respectively. Finally, the IVD tissue was further evaluated for the STING, p-TBK1, p-p65, TNF-α, Il-1β, IL-6, ACAN, Mmp13 expression confirm the siSTING@HP^{gel} effectiveness through prolonged STING pathway knockdown *in vivo*. IHC results showed that STING level in siSTING@HP^{gel} group was significantly lower than the signal observed in the other puncture groups at both 4 and 8 weeks and the expression of STING level was at a very low level similar to the control group (Fig. 8a), indicating the sustained STING silence by siSTING@HP^{gel}. IF was performed to test the p-TBK1 and p-p65 expression and the results showed similar trends with STING (Fig. S12a–**b**). Furthermore, the expression of TNF-α, Il-1β, IL-6 were significantly lower in the siSTING@HP^{gel} group than in other puncture groups (Fig. S13a–**c**). Importantly, the signal intensity of ACAN, an important indicator of ECM content, was significantly higher in siSTING@HP^{gel} group and the expression of Mmp13, an index of catabolism was lower than that observed in other puncture groups (Fig. 8b–**c**). These differences were further illustrated by semi-quantitative staining analysis (Fig. 8d–**f**, Fig. S12c–**d,** Fig. S13d–f). The results provided strong evidence to the effect of inhibiting IVD Inflammation and degeneration of the siSTING@HP^{gel} system *in vivo*.

Together, only siSTING administration had no therapeutic effect *in vivo* may duo to its shortcomings of low cellular uptake and rapid degradation. Although siSTING@PAMAM efficiently reduced STING expression, but short half-life and liquid therapy tended to leak from discs led to poor effective *in vivo*. HA played pivotal roles in many cellular and tissue functions, and single HA-CHO injection slightly inhibited IVD degeneration at early stages (4 W) as evidenced by excellent water retention [59]; however, its easy degradability limited its long-term application. Here, by formation of Schiff base between PAMAM and HA-CHO, we created a novel hydrogel that prolonged siSTING delivery and effectively regulated the IVD inflammation and

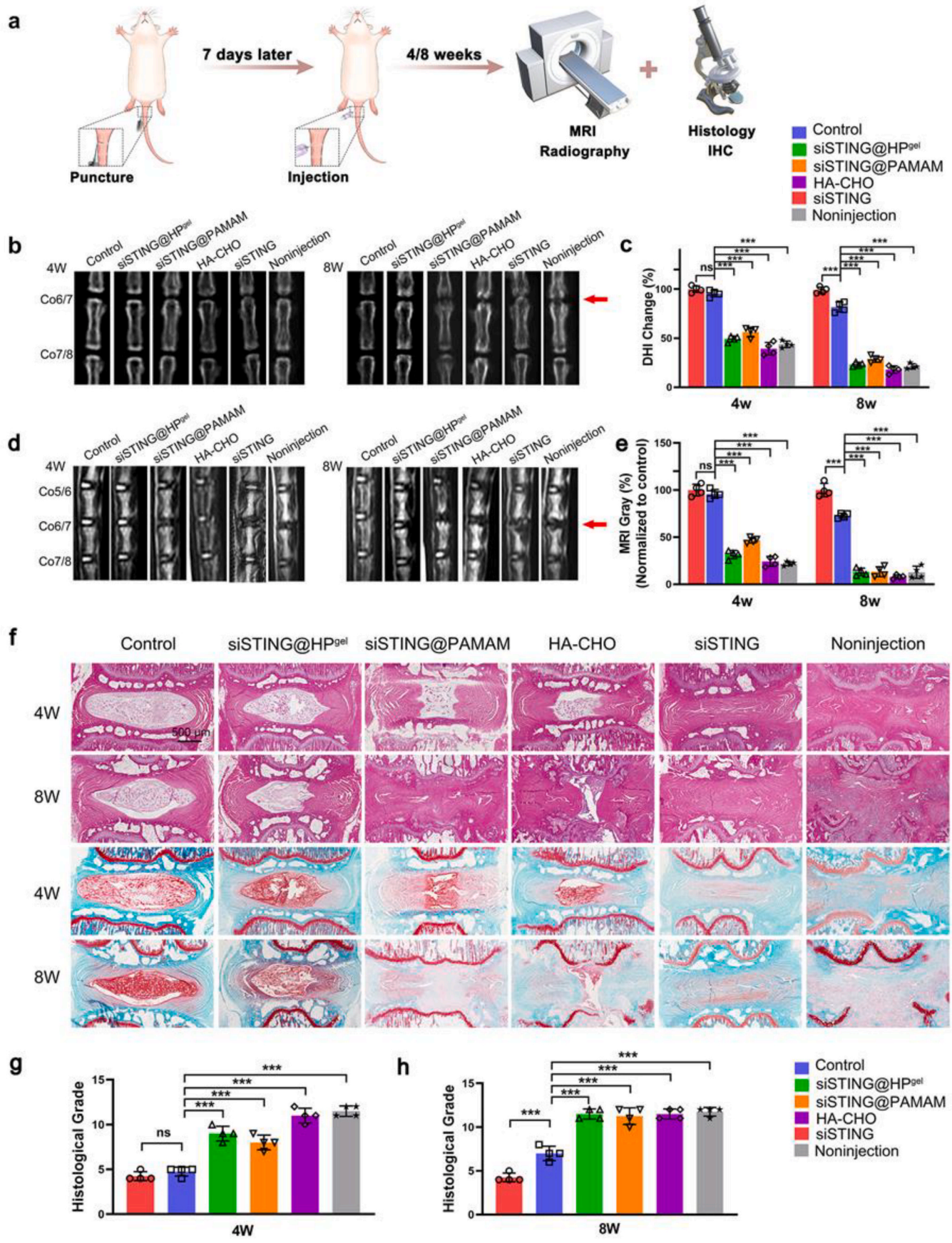

(caption on next page)

Fig. 7. siSTING@HP^{gel} significantly slowed the IVD degeneration progress in needle puncture-induced rat disc degeneration model. (**a**) Overview of animal experiments. (**b**) Representative X-ray images from different groups at 4 and 8 weeks. (**c**) Quantitative analysis of disc height index (DHI) measured on X-ray images (n = 4 individual discs in each group). (**d**) Representative MRI images from different groups at 4 and 8 weeks. (**e**) Quantitative analysis of T2 disc signal intensity calculated by Image J software and normalized to control group (n = 4 individual discs in each group). (**f**) Representative H&E and Safranin O and Fast Green staining images of different groups at different time points. (**g**–**h**) The histological grade of different groups at postoperative 4 and 8 weeks (n = 4 individual discs in each group). The values presented are the means ± SDs. ***$P < 0.001$, ns, not statistically significant. Statistical significance was assessed by one-way ANOVA with a post-hoc Tukey test. (For interpretation of the references to color in this figure legend, the reader is referred to the Web version of this article.)

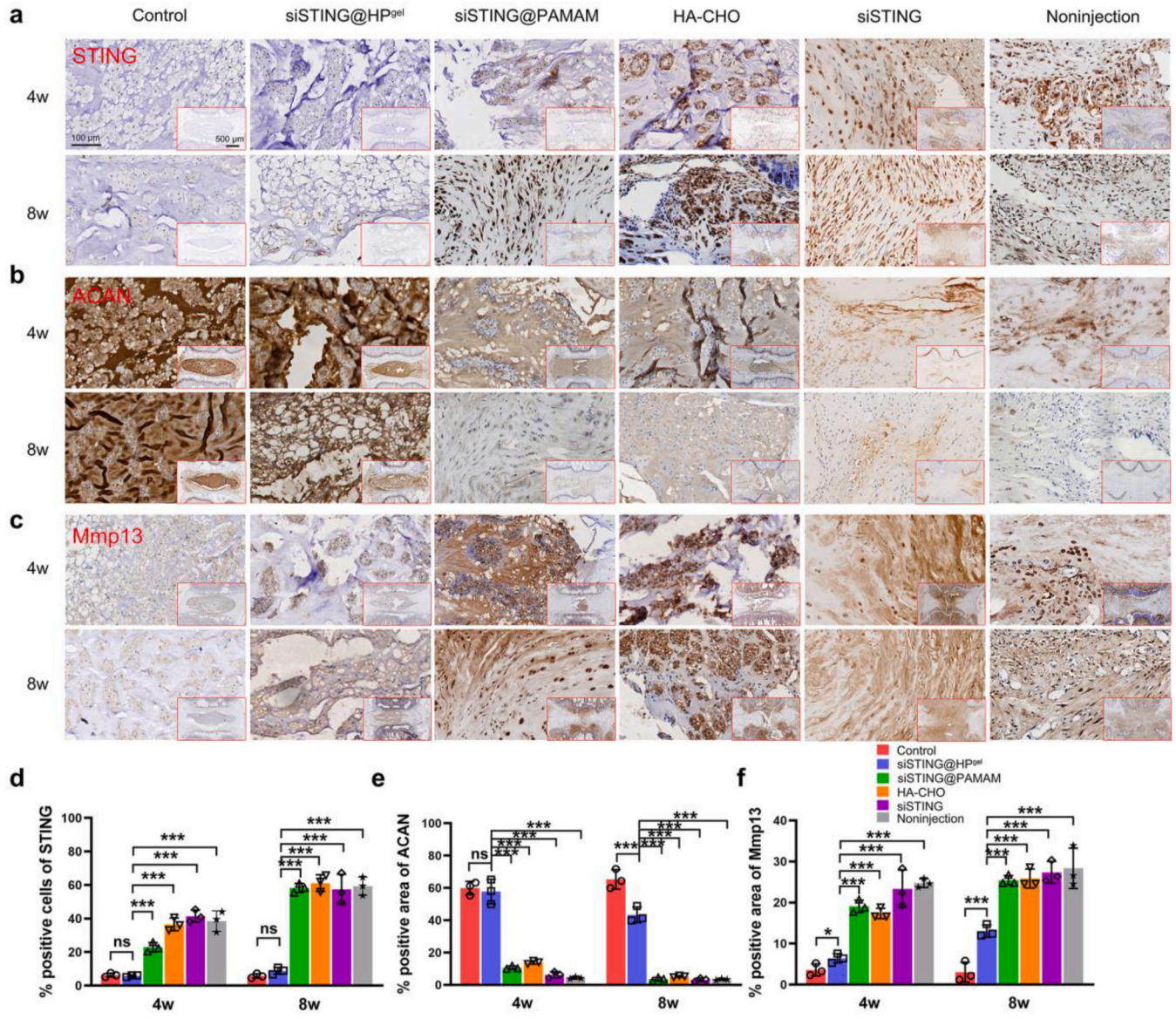

Fig. 8. Prolonged STING knockdown and therapeutic effect of siSTING@HP^{gel} *in vivo* by immunohistochemical (IHC) analysis. Representative IHC staining of STING (a), ACAN (b) and Mmp13 (c) in different groups at different time points. (d–f) The semi-quantitative analysis from IHC images in different groups at postoperative 4 and 8 weeks (n = 3 individual discs in each group). The values presented are the means ± SDs. *$P < 0.05$; ***$P < 0.001$; ns, not statistically significant. Statistical significance was assessed by one-way ANOVA with a post-hoc Tukey test.

degeneration *in vivo*.

4. Conclusions

In summary, we have identified the important function of STING in human degenerated IVD. ROS-induced cytosolic DNA leakage activates STING–NF–κB pathway and thus induces inflammation and degeneration in NP cells. Then we designed a novel, injectable, and self-healing siRNA delivery hydrogel through the mixture of aldehyde functionalized HA and PAMAM/siRNA polyplexes by formation of dynamic Schiff base bonds. Using the as-synthesized HP^{gel} hydrogel to efficiently transport siSTING and sustainedly silence STING expression in NP cells. Minimally invasive local injection of siSTING@HP^{gel} just once significantly slowed IVD inflammation and degeneration by prolonging STING knockdown in puncture-induced rat IVD degeneration model *in vivo*. We revealed STING pathway may be a potential therapeutic target for IVD degeneration and the hydrogel developed in this work showed a great potential for the treatment of IVD degeneration

that can be also applied to many other diseases by robust and prolonged gene delivery.

Declaration of competing interest

The authors declare no known competing financial interests in this work.

CRediT authorship contribution statement

Jiaxin Chen: Writing – original draft, Investigation, Methodology. **Haifeng Zhu:** Investigation, Methodology. **Yutao Zhu:** Data curation, Software. **Chenchen Zhao:** Investigation. **Shengyu Wang:** Investigation. **Yixin Zheng:** Methodology. **Ziang Xie:** Methodology. **Yang Jin:** Investigation, Data curation. **Honghai Song:** Formal analysis, Validation. **Linjun Yang:** Formal analysis, Validation. **Jin Zhang:** Supervision, Writing – review & editing. **Jiayong Dai:** Supervision, Funding acquisition, Writing – review & editing. **Zhijun Hu:** Supervision, Funding acquisition. **Huaiyu Wang:** Conceptualization.

Acknowledgements

The study was sponsored by National Natural Science Foundation of China (81672150, 51903050), Zhejiang medical and health science and technology project (2018KY117, 2019ZD041), Natural Science Foundation of Zhejiang Province of China (LQ20H160053), New talent in medical field of Zhejiang Province, and the fundamental research funds for the central universities (2019QNA7027).

Appendix A. Supplementary data

Supplementary data to this article can be found online at https://doi.org/10.1016/j.bioactmat.2021.08.003.

Data availability

All relevant data supporting the findings of this study are either included within the article and its Supplementary Information files or available upon request from the corresponding author.

References

[1] G.B. Andersson, Epidemiological features of chronic low-back pain, Lancet 354 (9178) (1999) 581–585.
[2] F. Balague, A.F. Mannion, F. Pellise, C. Cedraschi, Non-specific low back pain, Lancet 379 (9814) (2012) 482–491.
[3] G.E. Hicks, N. Morone, D.K. Weiner, Degenerative lumbar disc and facet disease in older adults: prevalence and clinical correlates, Spine 34 (12) (2009) 1301–1306.
[4] C.Q. Zhao, L.M. Wang, L.S. Jiang, L.Y. Dai, The cell biology of intervertebral disc aging and degeneration, Ageing Res. Rev. 6 (3) (2007) 247–261.
[5] L.J. Smith, N.L. Nerurkar, K.S. Choi, B.D. Harfe, D.M. Elliott, Degeneration and regeneration of the intervertebral disc: lessons from development, Dis Model Mech 4 (1) (2011) 31–41.
[6] M.F. Shamji, L.A. Setton, W. Jarvis, S. So, J. Chen, L. Jing, R. Bullock, R.E. Isaacs, C. Brown, W.J. Richardson, Proinflammatory cytokine expression profile in degenerated and herniated human intervertebral disc tissues, Arthritis Rheum. 62 (7) (2010) 1974–1982.
[7] G. Lang, Y. Liu, J. Geries, Z. Zhou, D. Kubosch, N. Sudkamp, R.G. Richards, M. Alini, S. Grad, Z. Li, An intervertebral disc whole organ culture system to investigate proinflammatory and degenerative disc disease condition, J Tissue Eng Regen Med 12 (4) (2018) e2051–e2061.
[8] S.B. Blanquer, D.W. Grijpma, A.A. Poot, Delivery systems for the treatment of degenerated intervertebral discs, Adv. Drug Deliv. Rev. 84 (2015) 172–187.
[9] D.L. Burdette, K.M. Monroe, K. Sotelo-Troha, J.S. Iwig, B. Eckert, M. Hyodo, Y. Hayakawa, R.E. Vance, STING is a direct innate immune sensor of cyclic di-GMP, Nature 478 (7370) (2011) 515–518.
[10] A. Ablasser, M. Goldeck, T. Cavlar, T. Deimling, G. Witte, I. Rohl, K.P. Hopfner, J. Ludwig, V. Hornung, cGAS produces a 2'-5'-linked cyclic dinucleotide second messenger that activates STING, Nature 498 (7454) (2013) 380–384.
[11] P. Gao, M. Ascano, Y. Wu, W. Barchet, B.L. Gaffney, T. Zillinger, A.A. Serganov, Y. Liu, R.A. Jones, G. Hartmann, T. Tuschl, D.J. Patel, Cyclic [G(2',5')pA(3',5')p] is the metazoan second messenger produced by DNA-activated cyclic GMP-AMP synthase, Cell 153 (5) (2013) 1094–1107.
[12] H. Ishikawa, G.N. Barber, STING is an endoplasmic reticulum adaptor that facilitates innate immune signalling, Nature 455 (7213) (2008) 674–678.
[13] C.K. Holm, S.B. Jensen, M.R. Jakobsen, N. Cheshenko, K.A. Horan, H.B. Moeller, R. Gonzalez-Dosal, S.B. Rasmussen, M.H. Christensen, T.O. Yarovinsky, F.J. Rixon, B.C. Herold, K.A. Fitzgerald, S.R. Paludan, Virus-cell fusion as a trigger of innate immunity dependent on the adaptor STING, Nat. Immunol. 13 (8) (2012) 737–743.
[14] J. Ahn, D. Gutman, S. Saijo, G.N. Barber, STING manifests self DNA-dependent inflammatory disease, Proc. Natl. Acad. Sci. U. S. A. 109 (47) (2012) 19386–19391.
[15] J. Ahn, T. Xia, H. Konno, K. Konno, P. Ruiz, G.N. Barber, Inflammation-driven carcinogenesis is mediated through STING, Nat. Commun. 5 (2014) 5166.
[16] K.W. Chung, P. Dhillon, S. Huang, X. Sheng, R. Shrestha, C. Qiu, B.A. Kaufman, J. Park, L. Pei, J. Baur, M. Palmer, K. Susztak, Mitochondrial damage and activation of the STING pathway lead to renal inflammation and fibrosis, Cell Metabol. 30 (4) (2019) 784–799, e5.
[17] W. Luo, Y. Wang, L. Zhang, P. Ren, C. Zhang, Y. Li, A.R. Azares, M. Zhang, J. Guo, K.B. Ghaghada, Z.A. Starosolski, K. Rajapakshe, C. Coarfa, Y. Li, R. Chen, K. Fujiwara, J.I. Abe, J.S. Coselli, D.M. Milewicz, S.A. LeMaire, Y.H. Shen, Critical role of cytosolic DNA and its sensing adaptor STING in aortic degeneration, dissection, and rupture, Circulation 141 (1) (2020) 42–66.
[18] A. Jauhari, S.V. Baranov, Y. Suofu, J. Kim, T. Singh, S. Yablonska, F. Li, X. Wang, P. Oberly, M.B. Minnigh, S.M. Poloyac, D.L. Carlisle, R.M. Friedlander, Melatonin inhibits cytosolic mitochondrial DNA-induced neuroinflammatory signaling in accelerated aging and neurodegeneration, J. Clin. Invest. 130 (6) (2020) 3124–3136.
[19] M. Sharma, S. Rajendrarao, N. Shahani, U.N. Ramírez-Jarquín, S. Subramaniam, Cyclic GMP-AMP synthase promotes the inflammatory and autophagy responses in Huntington disease, Proc. Natl. Acad. Sci. U. S. A. 117 (27) (2020) 15989–15999.
[20] C.H. Yu, S. Davidson, C.R. Harapas, J.B. Hilton, M.J. Mlodzianoski, P. Laohamonthonkul, C. Louis, R.R.J. Low, J. Moecking, D. De Nardo, K.R. Balka, D.J. Calleja, F. Moghaddas, E. Ni, C.A. McLean, A.L. Samson, S. Tyebji, C.J. Tonkin, C.R. Bye, B.J. Turner, G. Pepin, M.P. Gantier, K.L. Rogers, K. McArthur, P. J. Crouch, S.L. Masters, TDP-43 triggers mitochondrial DNA release via mPTP to activate cGAS/STING in ALS, Cell 183 (3) (2020) 636–649 e18.
[21] K.-P. Hopfner, V. Hornung, Molecular mechanisms and cellular functions of cGAS–STING signalling, Nat. Rev. Mol. Cell Biol. 21 (9) (2020) 501–521.
[22] T. Abe, G.N. Barber, Cytosolic-DNA-mediated, STING-dependent proinflammatory gene induction necessitates canonical NF-kappaB activation through TBK1, J. Virol. 88 (10) (2014) 5328–5341.
[23] N. Vo, H.Y. Seo, A. Robinson, G. Sowa, D. Bentley, L. Taylor, R. Studer, A. Usas, J. Huard, S. Alber, S.C. Watkins, J. Lee, P. Coehlo, D. Wang, M. Loppini, P. D. Robbins, L.J. Niedernhofer, J. Kang, Accelerated aging of intervertebral discs in a mouse model of progeria, J. Orthop. Res. 28 (12) (2010) 1600–1607.
[24] M.T. McManus, P.A. Sharp, Gene silencing in mammals by small interfering RNAs, Nat. Rev. Genet. 3 (10) (2002) 737–747.
[25] K.A. Whitehead, R. Langer, D.G. Anderson, Knocking down barriers: advances in siRNA delivery, Nat. Rev. Drug Discov. 8 (2) (2009) 129–138.
[26] A.K. Leung, Y.Y. Tam, P.R. Cullis, Lipid nanoparticles for short interfering RNA delivery, Adv. Genet. 88 (2014) 71–110.
[27] M. Zheng, Y. Liu, Y. Wang, D. Zhang, Y. Zou, W. Ruan, J. Yin, W. Tao, J.B. Park, B. Shi, ROS-responsive polymeric siRNA nanomedicine stabilized by triple interactions for the robust glioblastoma combinational RNAi therapy, Adv Mater 31 (37) (2019), e1903277.
[28] J. Zhuang, H. Gong, J. Zhou, Q. Zhang, W. Gao, R.H. Fang, L. Zhang, Targeted gene silencing in vivo by platelet membrane-coated metal-organic framework nanoparticles, Sci Adv 6 (13) (2020), eaaz6108.
[29] L. Frapin, J. Clouet, V. Delplace, M. Fusellier, J. Guicheux, C. Le Visage, Lessons learned from intervertebral disc pathophysiology to guide rational design of sequential delivery systems for therapeutic biological factors, Adv. Drug Deliv. Rev. 149–150 (2019) 49–71.
[30] G. Fontana, E. See, A. Pandit, Current trends in biologics delivery to restore intervertebral disc anabolism, Adv. Drug Deliv. Rev. 84 (2015) 146–158.
[31] M.K. Nguyen, O. Jeon, P.N. Dang, C.T. Huynh, D. Varghai, H. Riazi, A. McMillan, S. Herberg, E. Alsberg, RNA interfering molecule delivery from in situ forming biodegradable hydrogels for enhancement of bone formation in rat calvarial bone defects, Acta Biomater. 75 (2018) 105–114.
[32] L.A.L. Fliervoet, H. Zhang, E. van Groesen, K. Fortuin, N. Duin, K. Remaut, R. M. Schiffelers, W.E. Hennink, T. Vermonden, Local release of siRNA using polyplex-loaded thermosensitive hydrogels, Nanoscale 12 (18) (2020) 10347–10360.
[33] L.L. Wang, J.J. Chung, E.C. Li, S. Uman, P. Atluri, J.A. Burdick, Injectable and protease-degradable hydrogel for siRNA sequestration and triggered delivery to the heart, J. Contr. Release 285 (2018) 152–161.
[34] W. Chen, H. Chen, D. Zheng, H. Zhang, L. Deng, W. Cui, Y. Zhang, H.A. Santos, H. Shen, Gene-hydrogel microenvironment regulates extracellular matrix metabolism balance in nucleus pulposus, Adv. Sci. 7 (1) (2020) 1902099.
[35] S. Zhang, D. Huang, H. Lin, Y. Xiao, X. Zhang, Cellulose nanocrystal reinforced collagen-based nanocomposite hydrogel with self-healing and stress-relaxation properties for cell delivery, Biomacromolecules 21 (6) (2020) 2400–2408.
[36] C. Arakawa, R. Ng, S. Tan, S. Kim, B. Wu, M. Lee, Photopolymerizable chitosan-collagen hydrogels for bone tissue engineering, J Tissue Eng Regen Med 11 (1) (2017) 164–174.
[37] X. Cheng, L. Zhang, K. Zhang, G. Zhang, Y. Hu, X. Sun, C. Zhao, H. Li, Y.M. Li, J. Zhao, Circular RNA VMA21 protects against intervertebral disc degeneration through targeting miR-200c and X linked inhibitor-of-apoptosis protein, Ann. Rheum. Dis. 77 (5) (2018) 770–779.

[38] Q. Li, Y. Cao, C. Dang, B. Han, R. Han, H. Ma, J. Hao, L. Wang, Inhibition of double-strand DNA-sensing cGAS ameliorates brain injury after ischemic stroke, EMBO Mol. Med. 12 (4) (2020).
[39] S. Roberts, H. Evans, J. Trivedi, J. Menage, Histology and pathology of the human intervertebral disc, J Bone Joint Surg Am 88 (Suppl 2) (2006) 10–14.
[40] P. Tang, J.M. Gu, Z.A. Xie, Y. Gu, Z.W. Jie, K.M. Huang, J.Y. Wang, S.W. Fan, X. S. Jiang, Z.J. Hu, Honokiol alleviates the degeneration of intervertebral disc via suppressing the activation of TXNIP-NLRP3 inflammasome signal pathway, Free Radical Bio Med 120 (2018) 368–379.
[41] P. Tang, W.X. Chen, H.L. Gao, J.Y. Dai, Y. Gu, Z.A. Xie, X.F. Li, S.W. Fan, X.S. Jiang, Q. Lu, Z.J. Hu, Small molecule inhibitor of TAK1 ameliorates rat cartilaginous endplate degeneration induced by oxidative stress in vitro and in vivo, Free Radic. Biol. Med. 148 (2020) 140–150.
[42] C. Feng, M. Yang, M. Lan, C. Liu, Y. Zhang, B. Huang, H. Liu, Y. Zhou, ROS: crucial intermediators in the pathogenesis of intervertebral disc degeneration, Oxid Med Cell Longev 2017 (2017) 5601593.
[43] Z. Hu, X.L. Teng, T. Zhang, X. Yu, R. Ding, J. Yi, L. Deng, Z. Wang, Q. Zou, SENP3 senses oxidative stress to facilitate STING-dependent dendritic cell antitumor function, Mol Cell 81 (5) (2021) 940–952, e5.
[44] L. Tao, A. Lemoff, G. Wang, C. Zarek, A. Lowe, N. Yan, T.A. Reese, Reactive oxygen species oxidize STING and suppress interferon production, Elife 9 (2020), e57837.
[45] K. Wuertz, N. Vo, D. Kletsas, N. Boos, Inflammatory and catabolic signalling in intervertebral discs: the roles of NF-κB and MAP kinases, Eur. Cell. Mater. 23 (2012) 103–120.
[46] Q. Guo, X. Chen, J. Chen, G. Zheng, C. Xie, H. Wu, Z. Miao, Y. Lin, X. Wang, W. Gao, X. Zheng, Z. Pan, Y. Zhou, Y. Wu, X. Zhang, STING promotes senescence, apoptosis, and extracellular matrix degradation in osteoarthritis via the NF-κB signaling pathway, Cell Death Dis. 12 (1) (2021) 13.
[47] Y. Han, C.M. Zhou, H. Shen, J. Tan, Q. Dong, L. Zhang, S.J. McGowan, J. Zhao, G. A. Sowa, J.D. Kang, L.J. Niedernhofer, P.D. Robbins, N.N. Vo, Attenuation of ataxia telangiectasia mutated signalling mitigates age-associated intervertebral disc degeneration, Aging Cell 19 (7) (2020), e13162.
[48] S.M. Haag, M.F. Gulen, L. Reymond, A. Gibelin, L. Abrami, A. Decout, M. Heymann, F.G. van der Goot, G. Turcatti, R. Behrendt, A. Ablasser, Targeting STING with covalent small-molecule inhibitors, Nature 559 (7713) (2018) 269–273.
[49] J.J. Wu, L. Zhao, H.G. Hu, W.H. Li, Y.M. Li, Agonists and inhibitors of the STING pathway: potential agents for immunotherapy, Med. Res. Rev. 40 (3) (2019) 1117–1141.
[50] M.K. Nguyen, C.T. Huynh, A. Gilewski, S.E. Wilner, K.E. Maier, N. Kwon, M. Levy, E. Alsberg, Covalently tethering siRNA to hydrogels for localized, controlled release and gene silencing, Sci Adv 5 (8) (2019), eaax0801.
[51] C. Wang, M. Wang, T. Xu, X. Zhang, C. Lin, W. Gao, H. Xu, B. Lei, C. Mao, Engineering bioactive self-healing antibacterial exosomes hydrogel for promoting chronic diabetic wound healing and complete skin regeneration, Theranostics 9 (1) (2019) 65–76.
[52] F. Abedi-Gaballu, G. Dehghan, M. Ghaffari, R. Yekta, S. Abbaspour-Ravasjani, B. Baradaran, J.E.N. Dolatabadi, M.R. Hamblin, PAMAM dendrimers as efficient drug and gene delivery nanosystems for cancer therapy, Appl Mater Today 12 (2018) 177–190.
[53] H. Liu, C. Liu, L. Ye, D. Ma, X. He, Q. Tang, X. Zhao, H. Zou, X. Chen, P. Liu, Nanoassemblies with effective serum tolerance capability achieving robust gene silencing efficacy for breast cancer gene therapy, Adv Mater 33 (7) (2021) 2003523.
[54] A. Santos, F. Veiga, A. Figueiras, Dendrimers as pharmaceutical excipients: synthesis, properties, toxicity and biomedical applications, Materials 13 (1) (2019) 65.
[55] J. Bian, F. Cai, H. Chen, Z. Tang, K. Xi, J. Tang, L. Wu, Y. Xu, L. Deng, Y. Gu, W. Cui, L. Chen, Modulation of local overactive inflammation via injectable hydrogel microspheres, Nano Lett. 21 (6) (2021) 2690–2698.
[56] H.T.J. Gilbert, N. Hodson, P. Baird, S.M. Richardson, J.A. Hoyland, Acidic pH promotes intervertebral disc degeneration: acid-sensing ion channel-3 as a potential therapeutic target, Sci. Rep. 6 (2016) 37360.
[57] Y. Xiang, J. Liang, L. Liu, F. Wang, L. Deng, W. Cui, Self-nanoemulsifying electrospun fiber enhancing drug permeation, ACS Appl. Mater. Interfaces 11 (8) (2019) 7836–7849.
[58] C.W. Pfirrmann, A. Metzdorf, M. Zanetti, J. Hodler, N. Boos, Magnetic resonance classification of lumbar intervertebral disc degeneration, Spine 26 (17) (2001) 1873–1878.
[59] G. Abatangelo, V. Vindigni, G. Avruscio, L. Pandis, P. Brun, Hyaluronic acid: redefining its role, Cells 9 (7) (2020) 1743.